Journal of Computer Assisted Tomography
11(3):369–377, May/June

Motion Artifact Suppression Technique (MAST) for MR Imaging

Pradip M. Pattany, Jeffrey J. Phillips, Lee C. Chiu, James D. Lipcamon, Jeffrey L. Duerk, James M. McNally, and Surya N. Mohapatra

Abstract: A technique has been developed that significantly improves the image resolution and reduces motion artifacts in conventional two-dimensional Fourier transform and three-dimensional Fourier transform magnetic resonance imaging sequences. Modifications on the gradient waveforms completely refocus the transverse magnetization at the echo time, regardless of the motion occurring between the time of the 90° radiofrequency excitation and the echo time (within-view). This accomplishes suppression of motion artifacts and regains the signal from flowing blood and CSF. Images of the head, abdomen, chest, and spine are reproduced which show the increase in signal and anatomical detail that would otherwise be degraded and lost in artifact noise. This technique has reduced the practical difficulty of obtaining clinically diagnostic T2-weighted abdominal images. It also has allowed diagnostic quality T1- and T2-weighted images to be obtained with one acquisition per view, thus reducing the total scan time. **Index Terms:** Magnetic resonance imaging, techniques—Artifacts—Magnetic resonance imaging, physics.

Various techniques have been tried to reduce motion artifacts and produce diagnostically useful T2-weighted magnetic resonance (MR) images. With respiratory gating, the data are collected during the minimum motion period (end expiration) (1). There is no major displacement of the object being scanned between each view, thereby achieving view-to-view consistency (Fig. 1a). However, gating techniques fail to consider the random motion occurring between the 90° radiofrequency (RF) excitation and data collection period (within-view motion, Fig. 1b). Incomplete rephasing of magnetization at the center of the read gradient and at the end of the slice select gradient results in artifacts.

Respiratory ordered phase encoding techniques scan the central views during minimum motion and outer views during maximum motion (2,3). This reduces artifacts but similarly does not take into consideration random phase errors resulting from incomplete rephasing due to motion occurring within the view. For T1-weighted images, short echo time (TE)/repetition time (TR) sequences are used with multiple acquisitions (4). This technique averages the random phases which leads to artifact reduction without any regard to view-to-view displacement of the object and within-view motion. In spite of all the aforementioned limitations, the highly T2-dependent spin echo (SE) pulse sequence is presently widely used for screening purposes.

A general solution has been derived that refocuses the magnetization in the imaging plane and zeroes the within-view random phase terms due to respiratory, cardiac, involuntary ocular and peristaltic motions, as well as to blood and CSF flow. As a result, these motion artifacts are dramatically reduced.

MATERIALS AND METHODS

Any physiologic motion occurring within-view along the read and slice select directions leads to incomplete rephasing at the center of the conventional data collection (read) gradient and at the end of the conventional slice select gradient. This addi-

From the Department of Radiology, Harbor–University of California at Los Angeles Medical Center, Torrance, CA (J. J. Phillips, L. C. Chiu, and J. D. Lipcamon), and the Picker International Clinical Science Center, Cleveland, OH (P. M. Pattany, J. L. Duerk, J. M. McNally, and S. N. Mohapatra). Address correspondence and reprint requests to Dr. L. C. Chiu at Department of Radiology, Harbor–UCLA Medical Center, 1000 West Carson Street, Torrance, CA 90502, U.S.A.

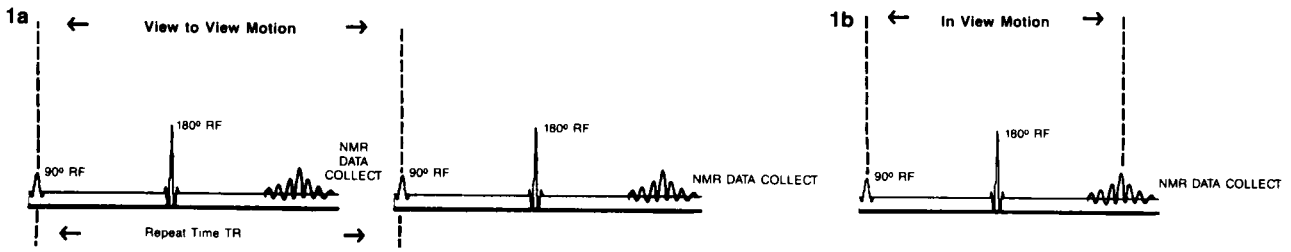

FIG. 1. a: Minimizing displacement of the anterior abdominal wall between the initiation of imaging sequences (views) is the principle behind respiratory gating. **b:** Physiologic motion occurring between the time of the 90° radiofrequency (RF) pulse and data collection (within-the-view) results in random phase errors and image degradation.

tional random phase term in two-dimensional Fourier transform (2DFT) and three-dimensional Fourier transform (3DFT) imaging leads to displacement of the object signal (Eq. 1, Appendix) and results in artifacts in the phase encode direction. Motion along the phase encode direction does not contribute significantly to these artifacts because of the relatively short time (3 ms) for which the phase encoding gradient is applied. The artifacts are more prominent in 3DFT where the phase encoding is applied in two axes.

The physical principles of SE technique (Fig. 2a) have been well described (5,6). The standard 2DFT read and slice select gradients for multislice SE sequences can be modified (Fig. 2b) to reduce significantly the artifacts from physiologic motion. The solution to a set of simultaneous equations determines the parameters for the gradient profile necessary to refocus moving material with constant velocity, acceleration, and pulsatility. The mathematical formulas on which these modifications are based are presented in detail in the Appendix.

The MR images were obtained on the Picker 0.5 T VISTA MR 2055 static and mobile systems. Subjects included normal volunteers and patients referred to Picker Clinical Science Center and to Harbor–University of California at Los Angeles for diagnostic imaging. Informed consents were obtained in the latter group.

All anatomical areas where physiological motion exists were imaged with the technique to investigate its clinical utility. In all instances, images with conventional SE techniques were obtained at the same time, as a control. Motion artifact suppression technique (MAST) and conventional SE sequences used identical scanning parameters. For the brain, 1 cm sections with one excitation, 256 × 256 matrix, TR of 2,000 ms and TE of 80–100 ms were obtained. Images of the orbits and cervical spine using surface coils and lumbar spine with body coil were produced using 5–10 mm sections, one to two excitations, 256 × 256 matrix, TR of 2,000 ms, and TE of 80–100 ms. The T2-weighted abdominal imaging was accomplished with 1 cm sections, two averages, 256 × 256 matrix, TR of 1,600–2,000 ms, and TE of 100 ms.

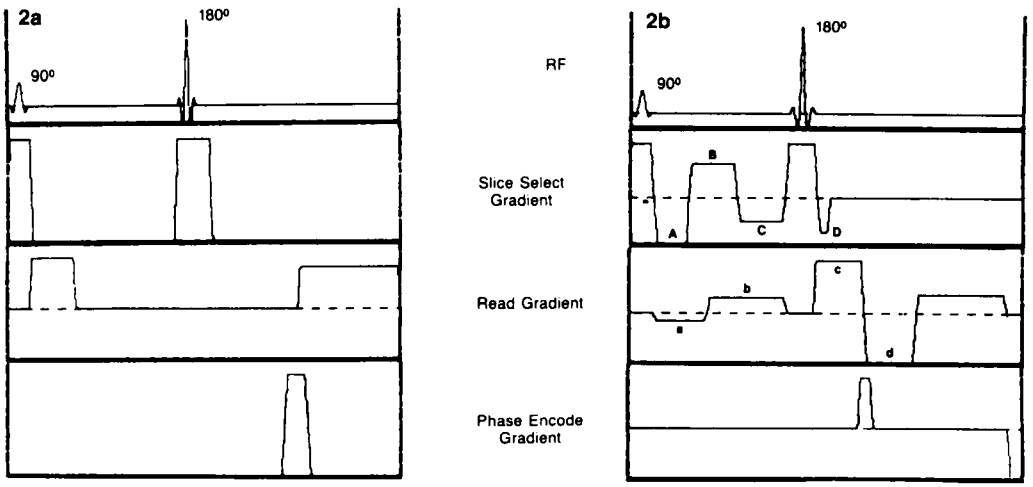

FIG. 2. a: Gradient profile for standard spin echo sequence shows the relationship of the 90° and 180° radiofrequency (RF) pulses and the applied gradients. **b:** Four additional, mathematically derived gradient pulses are applied in the slice select (A–D) and read (a–d) directions in motion artifact suppression technique (MAST) TE 100 sequences. Significant refocusing of magnetization in the imaging plane is accomplished. See text for explanation.

Abdomen

An imaging area that benefits substantially from motion suppression is the upper abdomen. Up to now, inferior image quality, particularly in the left upper quadrant, has relegated MR to a secondary role in the majority of clinical settings. Yet, several investigators have shown superior sensitivity with MR in detection of liver pathology (4,7,8). The modality has also demonstrated superior specificity compared with CT for some common adrenal and hepatic lesions (9,10). By improved signal-to-noise and demonstration of anatomic detail, it is reasonable to expect "artifact-suppressed" MR to assume an important position in abdominal imaging.

With no increase in imaging time, no additional equipment, and little appreciable loss in spatial resolution as compared with short TE (26 ms) sequences, MAST has provided high quality T2-weighted images. The majority of comparisons to date have been with high resolution CT and conventional SE T1- and T2-weighted MR images. Figure 3 shows CT and MR of a patient with treated hydatid liver disease. The findings relate to the collapsed cysts in an extensively involved right hepatic lobe. The T1-weighted image, while demonstrating good overall resolution and lesion-to-liver contrast, fails to show any of the complex detail in the cystic area itself. Comparison of the MAST image with the SE T2-weighted image shows far superior anatomic detail within the liver as well as within the spleen and stomach. Portal venous branches are clearly seen.

Other retroperitoneal structures, most notably the pancreas, have also shown superior resolution with the MAST protocol. We have obtained image quality comparable with that of short TE, T1-

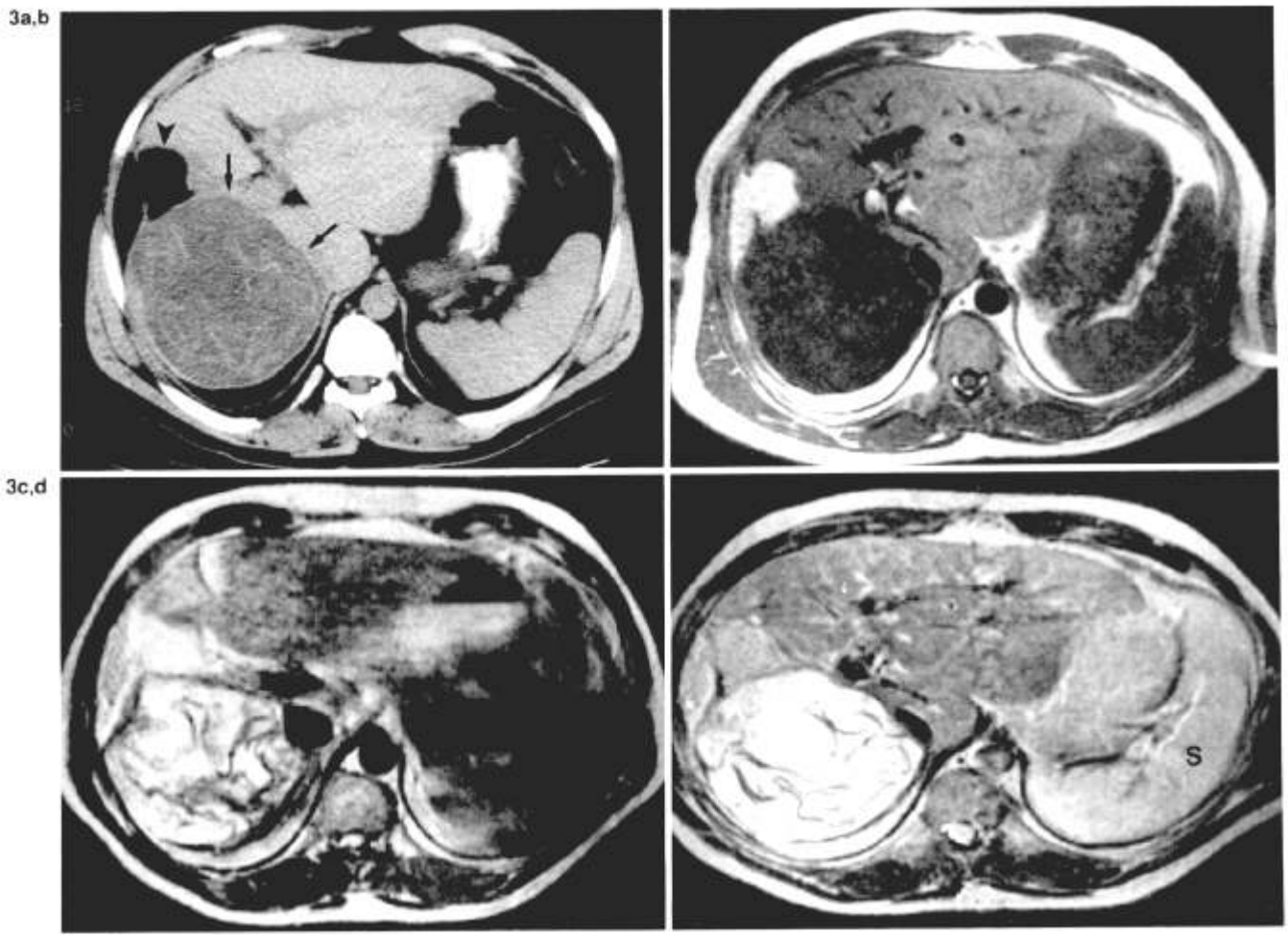

FIG. 3. a: CT of treated hydatid cyst of the liver (arrows). Collapsed appearance is probably the effects of 9 months of antihelminthic therapy. There had been previous surgical intervention (arrowhead). **b:** T1-weighted (TR 600/TE 26) SE image at same level. **c:** A standard T2-weighted (TR 1,800/TE 100) SE sequence demonstrates the extensive artifacts and signal loss typically associated with long TR images in upper abdomen. **d:** Motion artifact suppression technique (MAST) image (TR 1,800/TE 100) at the same level, acquired in the same amount of time as (c). Note improved detail within cystic lesion and within spleen (S). This detail is absent on the routine T2-weighted sequence. Portal branches are also well visualized.

weighted sequences with 7 and 10 mm thick sections and two averages (Fig. 4).

Pelvis

The clinical utility of T2-weighted images in the pelvis is well recognized. Display of uterine zonal anatomy and superior contrast between tumors and surrounding normal tissue are clear advantages of long TE/TR sequences (11). Motion artifacts from the rectosigmoid have been described as contributing to decreased resolution within the pelvis and have prompted the recommendation of fasting plus glucagon administration to improve image quality (12). Although this represents a potentially problematic area, we have noted the greatest benefit from motion suppression to lie in the middle and upper abdomen. Long TE/TR sagittal imaging through the pelvis routinely includes visualization of middle and upper abdominal structures including liver, spleen, and kidneys. Conventional TE 100 SE sequences suffer from significant artifacts and signal loss in these areas. Use of MAST has resulted in retrieval of useful information from the upper abdomen, particularly the liver (Fig. 5). We see this as a definite advantage in instances where this has clinical relevance such as in detection of metastatic disease.

Head and Neck

Motion artifacts in the CNS, orbits, and head and neck have posed less of a significant problem for MR imaging. Nevertheless, flowing CSF, involuntary eye motion, and swallowing often result in loss of signal and noticeable "ghosting." It is for these reasons that MAST images show notable improvements when compared with routine SE sequences.

Routine use of T2-weighted imaging with MAST has shown clearer definition of the interface between the brain stem, exiting cranial and cervical nerve roots, and the CSF. Figures 6 and 7 show images through the brain stem region of normal volunteers using routine SE sequences and MAST for comparison. There is brighter and more uniform signal from the CSF surrounding the brain stem and adjacent structures on the MAST images resulting in improved resolution. Signal loss (flow void) routinely seen within the aqueduct on standard SE sequences is consistently recovered with MAST. The modifications made on the read and slice select gradients refocus material flowing with constant ve-

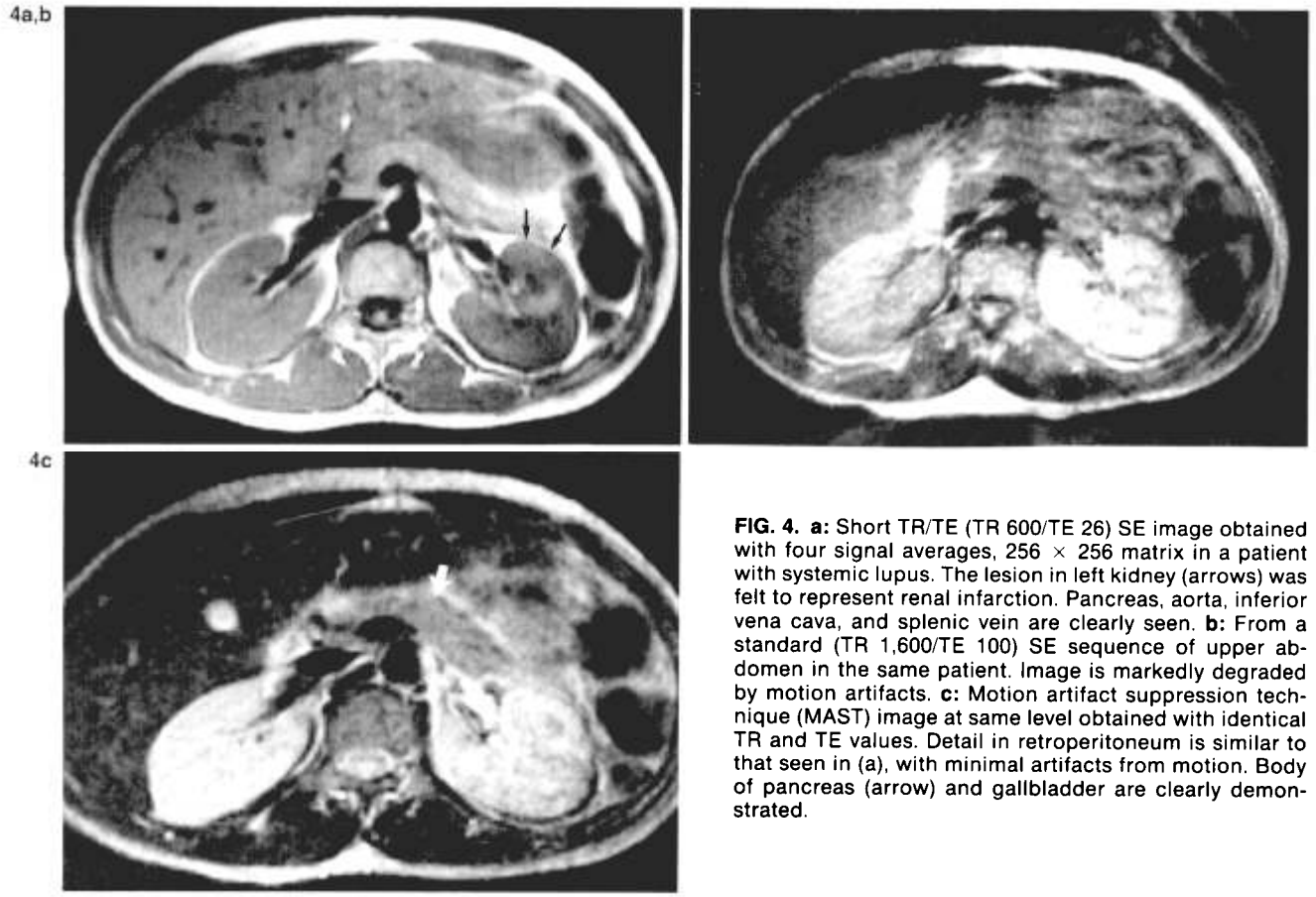

FIG. 4. a: Short TR/TE (TR 600/TE 26) SE image obtained with four signal averages, 256 × 256 matrix in a patient with systemic lupus. The lesion in left kidney (arrows) was felt to represent renal infarction. Pancreas, aorta, inferior vena cava, and splenic vein are clearly seen. **b:** From a standard (TR 1,600/TE 100) SE sequence of upper abdomen in the same patient. Image is markedly degraded by motion artifacts. **c:** Motion artifact suppression technique (MAST) image at same level obtained with identical TR and TE values. Detail in retroperitoneum is similar to that seen in (a), with minimal artifacts from motion. Body of pancreas (arrow) and gallbladder are clearly demonstrated.

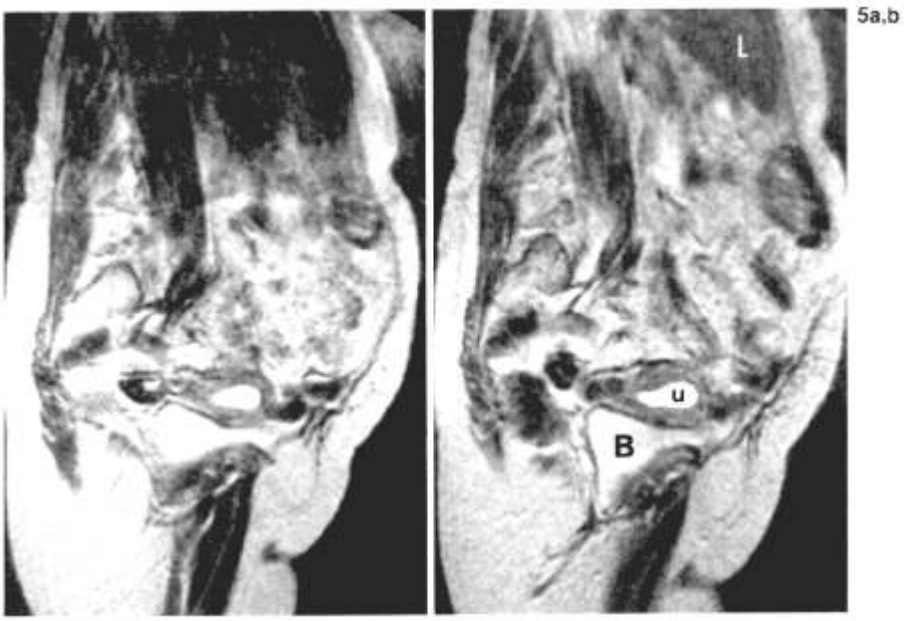

FIG. 5. a: Sagittal image through the midabdomen and pelvis (TR 1,800/TE 100) in a middle-aged woman with menorrhagia. Physiologic motion creates artifacts and signal displacement in upper two-thirds of abdomen. **b:** Identical SE sequence using motion artifact suppression technique (MAST) shows reduction of ghosting artifact and improved resolution in region of liver (L) and abdominal cavity. B, bladder; u, uterine cavity.

locity, acceleration, and pulsatility. This results in visualization of the flowing CSF within the aqueduct. We have found that suppression of artifacts from eye motion and swallowing has improved overall image quality. Figure 7 illustrates the achievable reduction in these motion-related artifacts.

Spine

Comparisons between sagittal MAST images of the spine and routine long TR/TE sequences have shown some notable differences. In the lumbar area the reduction of artifacts from the abdomen anterior to the spine with horizontal phase encoding has resulted in improved anatomic detail within the spinal canal (Fig. 8). The aliasing artifact seen with vertical phase encoding is eliminated through use of horizontal phase encoding.

In both the cervical and lumbar spines, enhancement of signal from flowing CSF eliminates or drastically reduces phase shift (ghosting) artifacts from the CSF and more clearly defines the boundaries of the subarachnoid space (Fig. 9). Also, the reduction of motion artifacts from swallowing is noticeable, resulting in better quality images.

Chest

There are multiple complex factors contributing to motion within the chest and mediastinum. Long TE and long TR sequences have generally been unsatisfactory in these areas. The MAST images in the chest are not free of image-degrading motion artifacts. Nevertheless, T2-weighted images are frequently of benefit in the characterization of abnormal tissue and a description of the observable

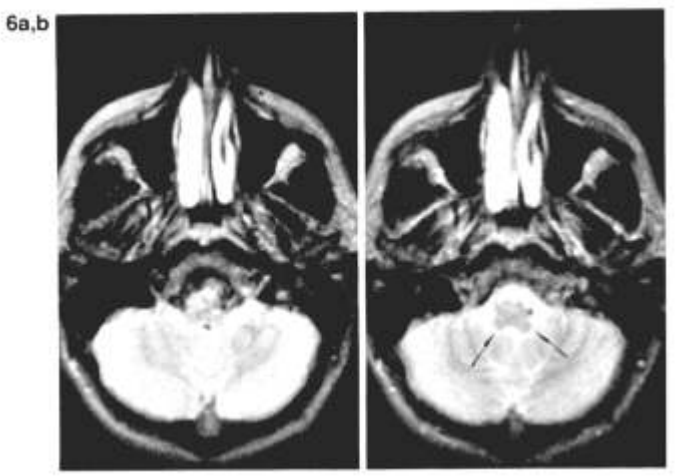

FIG. 6. a: Axial (TR 2,000/TE 100) standard SE image. There is noticeable "ghosting" from pulsatile blood flow and relatively poor resolution in region of lower brain stem. **b:** Motion artifact suppression technique (MAST) image at same level. Diminished motion artifacts and uniform signal from the CSF help in clearly delineating the margins of the brain stem (arrows).

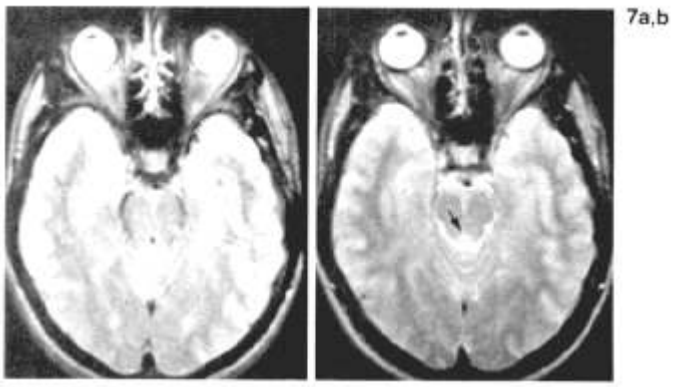

FIG. 7. a: Axial (TR 2,000/TE 100) SE image at level of orbits. Involuntary eye movements result in ghosting artifact. **b:** With motion artifact suppression technique (MAST) there are less artifacts and the CSF–brain stem interface is more clearly demonstrated. Note that CSF signal has been recovered from within aqueduct (arrow) (see text).

improvements with the MAST technique is in order.

When compared with SE T2-weighted images, we have noted not only the presence of intermediate-intensity echoes within the major vessels of the mediastinum, but also an accentuation (increased intensity) of the mediastinal fat and vascular boundaries (see Fig. 10). The patient presented with cervical adenopathy and an anterior mediastinal mass that was later proven to be Hodgkin lymphoma. Although the contrast between lesion and normal mediastinum is more evident on the SE T2-weighted image, detail within the mediastinum itself is greater in the MAST image. Note on the latter the clear demarcation between superior vena cava and ascending aorta and between vascular structures and the main stem bronchi. We have been able to reduce artifacts further using four averages with a 128 × 128 matrix. Further work, however, remains to be done in this area.

DISCUSSION

Efforts at reducing motion artifacts in the body have dealt, in large part, with attempting to achieve view-to-view consistency during data collection and by signal averaging. The former techniques ignore motion occurring within the view. Incomplete rephasing of the transverse magnetization will result in random phase errors and image artifacts. Gating techniques also generally demand at least a 60% increase in scan time. Multiple averaging techniques are limited to T1-weighted images and may be less sensitive in the detection of hepatic lesions and other pathology.

In the imaging plane MAST rephases magnetization and eliminates random phase terms within the view due to the various forms of body motion. This accomplishes significant reduction in motion artifacts without the expenditure of additional time and with as few as one acquisition per view. Clinical applications to date show substantial benefit from

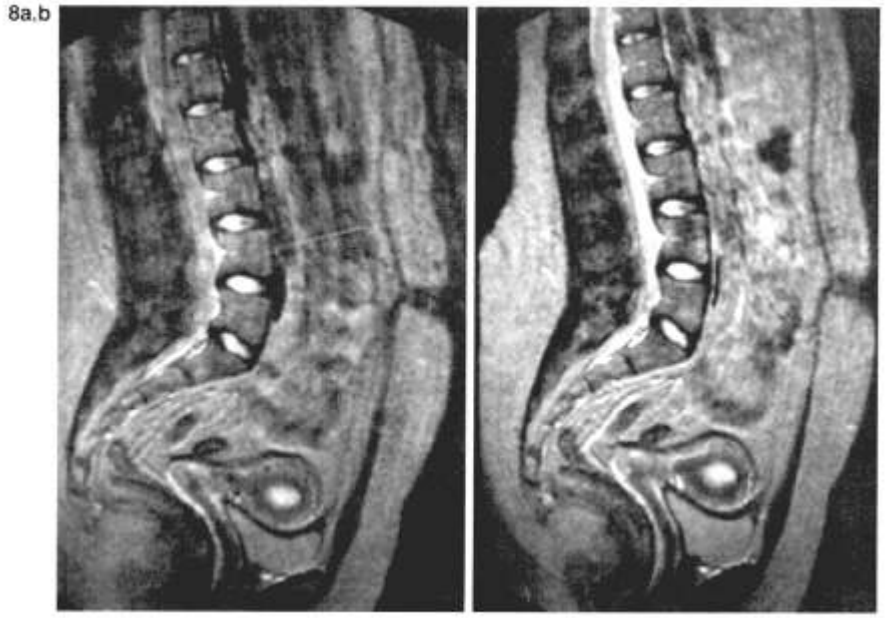

FIG. 8. a: Spin echo image through lumbar spine in a normal volunteer. Peristaltic motion results in propagation of artifacts across the spinal canal, obscuring anatomic detail. **b:** Motion artifact suppression technique (MAST) image, near-identical scanning parameters (TR 2,000/TE 100). There is noticeable reduction in motion artifacts, resulting in improved resolution within spinal canal.

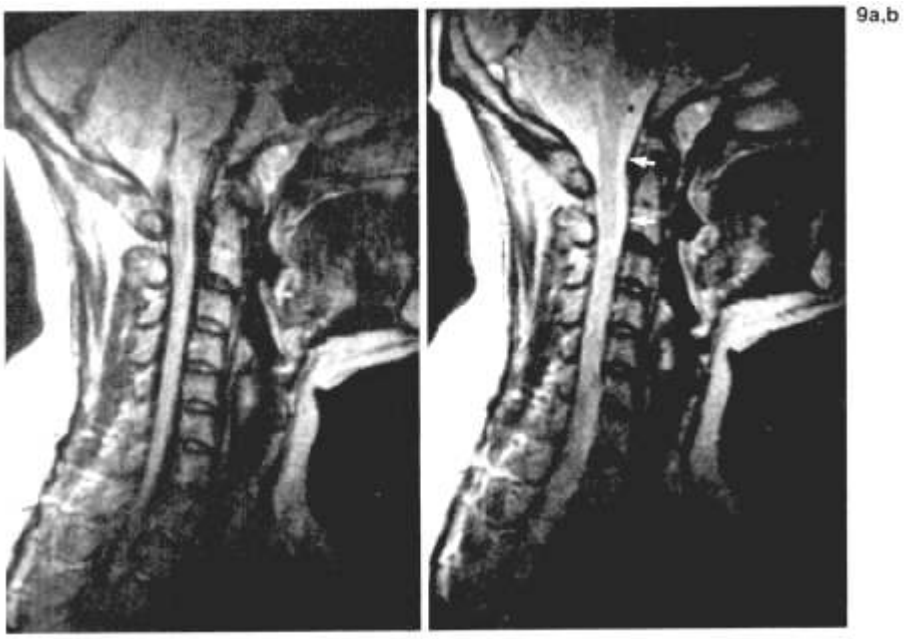

FIG. 9. a: Sagittal TR 2,000/TE 80 SE image of cervical spine. **b:** Motion artifact suppression technique (MAST) image shows reduction of motion artifacts from swallowing and uniform signal from CSF (arrows), giving better delineation of upper cord and brain stem. Image was obtained with one acquisition.

within-view motion suppression in upper abdominal imaging. Significant signal degradation and artifacts from respiratory, cardiac, and peristaltic motions have generally resulted in nondiagnostic image quality on T2-weighted scans. Comparable images using MAST have demonstrated markedly improved detail within the liver, spleen, and retroperitoneum. Sagittal abdominal and pelvic images similarly have shown noticeable gain in signal intensity and detail in the areas of maximum physiologic motion. This statement also applies to sagittal images of the spine, which might otherwise be obscured by artifact noise. Sources of motion in the head and neck include involuntary eye motion and swallowing, as well as blood and CSF flow. Application of MAST has resulted in reduction of motion artifact and enhancement of signal from CSF and vascular structures. Overall image quality is improved with an increase in diagnostically useful information. The need for gating techniques to compensate for CSF motion effects is eliminated or reduced.

In conventional SE technique, flowing blood is not refocused, resulting in a signal void within the vessels. With MAST, signal from moving blood is refocused and appears as bright or intermediate signal intensity. Work is currently being undertaken regarding the potential usefulness of this finding for blood flow quantification. Overall, MAST provides the flexibility to obtain diagnostic SE T2-weighted

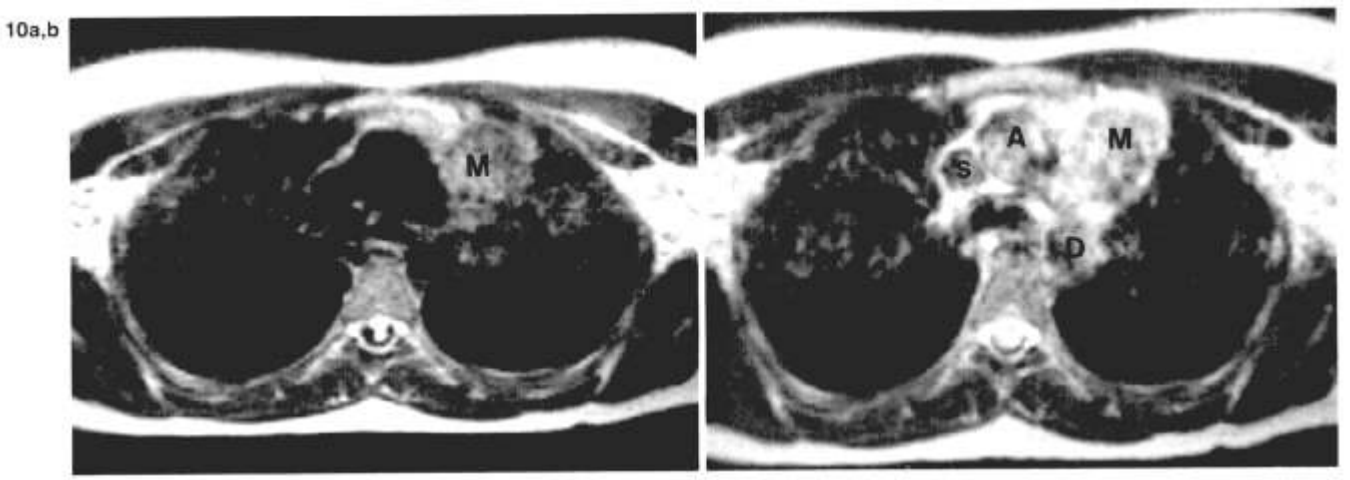

FIG. 10. a: T2-weighted SE image (TR 2,000/TE 100) near level of carina. Mass (M) in left anterior thorax is from Hodgkin lymphoma. **b:** Motion artifact suppression technique (MAST) image at same level. Note intermediate signal intensity within the great vessels and enhanced interfaces within the mediastinum. M, mass; S, superior vena cava; A, ascending aorta; D, descending aorta.

images in regions of greatest physiological motion. Efforts are being made to similarly modify other imaging sequences to obtain artifact-suppressed images.

APPENDIX

The phase of the excited packet of magnetization with time-varying imaging gradient pulses is shown in the equation below.

$$S(t_x,t_y) = \iint \tilde{\rho}(x,y) e^{-j2\pi\gamma[\int \vec{G}_x(t_x)\vec{x}(t_x)dt_x + \int \vec{G}_y(t_y)\vec{y}(t_y)dt_y]}\, dx\, dy \quad (1a)$$

$$S(t_x,t_y) = \iint \tilde{\rho}(x,y) e^{-j2\pi\gamma[\int \vec{G}_x dt_x(\vec{x} + \vec{V}_x t_x + 1/2\vec{A}_x t_x^2 + 1/6\vec{P}_x t_x^3)dt_x + \int \vec{G}_y(t_y)(\vec{y} + \vec{V}_y t_y + 1/2\vec{A}_y t_y^2 + 1/6\vec{P}_y t_y^3)dt_y]}\, dx\, dy \quad (1b)$$

$$\tilde{\rho}(x,y) = \int \bar{\rho}(x,y,z) e^{-j2\pi\gamma\int \vec{G}_z(t_z)\vec{z}(t_z)dt_z} dz \quad (1c)$$

$$\bar{\rho}(x,y,z) = \rho(x,y,z)(1 - e^{-T_R/T_1(x,y,z)}) \quad (1d)$$

where $S(t_x,t_y)$ is the signal in the transverse plane.

Partial volume effects due to finite slice thickness are within $p(x,y)$ as a result of integration along dz.

To obtain a maximum signal in the $X-Y$ plane following a selective 90° RF pulse,

$$e^{-j2\pi\gamma\int \vec{G}_z(t_z)\vec{z}(t_z)dt_z} = e^{-j2\pi\phi_z(t_z)} = 1.0 \quad (2)$$

$$\phi_z(t_z) = \gamma\int \vec{G}_z(t_z)\vec{z}(t_z)dt_z = 0.0 \quad (3)$$

Where ϕ is the phase of magnetization packet at time t; γ is the gyromagnetic ratio; $G(t)$ is the gradient at time t; $z(t)$ is the position of the magnetization packet at time t.

The $z(t)$ term can be expanded by a Taylor series:

$$\vec{z}(t_z) = \vec{z} + \frac{\Sigma t_2^j \vec{z}_0^{(j)}}{j!} \quad (4)$$

Where $z_0^{(j)}$ is the j^{th} differential of z.

Each of the terms of the expanded $z(t)$ expression shown in Eq. 4 is integrated separately using Eq. 3 and brought to zero at the end of the slice select. Similar expansion along the other axes requires that the phase be brought to zero at the center of data collect or read gradient.

$$\phi_z(t_z) = \gamma\int \vec{G}_z(t_z)\vec{z}(t_z)dt_z \quad (5a)$$

$$\phi_z(t_z) = \gamma\int \vec{G}_z(t_z)[\vec{z} + \vec{V}_z t_z + 1/2\vec{A}_z t_z^2 + 1/6\vec{P}_z t_z^3 + \ldots]dt_z \quad (5b)$$

Therefore, for complete rephasing

$$\int \vec{G}_z(t_z)dt_z = C_0 = 0.0 \quad (6a)$$

$$\int \vec{G}_z(t_z)t_z dt_z = C_1 = 0.0 \quad (6b)$$

$$1/2\int \vec{G}_z(t_z)t_z^2 dt_z = C_2 = 0.0 \quad (6c)$$

$$1/6\int \vec{G}_z(t_z)t_z^3 dt_z = C_3 = 0.0 \quad (6d)$$

$$1/n!\int \vec{G}_z(t_z)t_z^n dt_z = C_n = 0.0 \quad (6e)$$

The above set of simultaneous equations can be solved by using the matrix equation shown below:

$$\begin{bmatrix} 1/0!\int_{A_1}^{B_1} t_z^0 dt_z & 1/0!\int_{A_2}^{B_2} t_z^0 dt_z & 1/0!\int_{A_3}^{B_3} t_z^0 dt_z & 1/0!\int_{A_4}^{B_4} t_z^0 dt_z \\ 1/1!\int_{A_1}^{B_1} t_z^1 dt_z & 1/1!\int_{A_2}^{B_2} t_z^1 dt_z & 1/1!\int_{A_3}^{B_3} t_z^1 dt_z & 1/1!\int_{A_4}^{B_4} t_z^1 dt_z \\ 1/2!\int_{A_1}^{B_1} t_z^2 dt_z & 1/2!\int_{A_2}^{B_2} t_z^2 dt_z & 1/2!\int_{A_3}^{B_3} t_z^2 dt_z & 1/2!\int_{A_4}^{B_4} t_z^2 dt_z \\ 1/3!\int_{A_1}^{B_1} t_z^3 dt_z & 1/3!\int_{A_2}^{B_2} t_z^3 dt_z & 1/3!\int_{A_3}^{B_3} t_z^3 dt_z & 1/3!\int_{A_4}^{B_4} t_z^3 dt_z \\ \downarrow & \downarrow & \downarrow & \downarrow \\ \frac{1}{(n-1)!}\int_{A_1}^{B_1} t_z^{(n-1)} dt_z & \frac{1}{(n-1)!}\int_{A_2}^{B_2} t_z^{(n-1)} dt_z & \frac{1}{(n-1)!}\int_{A_3}^{B_3} t_z^{(n-1)} dt_z & \frac{1}{(n-1)!}\int_{A_4}^{B_4} t_z^{(n-1)} dt_z \end{bmatrix} \begin{bmatrix} G_{(1)} \\ G_{(2)} \\ G_{(3)} \\ G_{(4)} \\ G_{(n)} \end{bmatrix} = \begin{bmatrix} S_{(0)} \\ S_{(1)} \\ S_{(2)} \\ S_{(3)} \\ S_{(n-1)} \end{bmatrix} - \begin{bmatrix} U_{(0)} \\ U_{(1)} \\ U_{(2)} \\ U_{(3)} \\ U_{(n-1)} \end{bmatrix}$$

Where A_i is the starting point of i^{th} unknown gradient pulse; B_i is the endpoint of i^{th} unknown gradient pulse. In matrix notation

$$PG = S - U$$

$$PG = W$$

where P is $n \times n$ matrix of 0 to $n - 1$ moments of additional n gradient lobes; G is $n \times 1$ matrix of unknown gradient amplitudes; U is $n \times 1$ moments of known gradients; S is $n \times 1$ desired moments of total gradient waveform; W is difference of S and U matrices, i.e., required moments of additional lobes.

The right hand matrix U is the summation of the integral of known gradients G.

The second right hand side matrix S allows the moments of the total gradient waveform to be specified to achieve the desired artifact reduction. The G matrix is the unknown gradient amplitudes to be calculated. The left square matrix P contains all the integral terms of the various moments at specified times for the unknown gradients.

To rephase expansion terms of order zero (static) through three (pulsatility), four unknown gradient pulses are applied at given time intervals in a gradient profile. The amplitude of the read gradient during data sampling is set to give the correct field of view. The four pulses are applied at given times as shown in Fig. 2b.

The 4×4 P matrix is solved in terms of the specified time intervals. It is then inverted.

The product of P^{-1} and W will solve for the amplitudes of the unknown pulses (a, b, c, and d). This results in complete rephasing of static material, material with constant velocity, constant acceleration, and constant pulsatility. Similarly the method can be applied to the slice select direction since the amplitudes of the gradient pulses applied during the RF are known to give a correct slice thickness (refer to Fig. 2b).

Four unknown gradient pulses (A, B, C, and D) are applied as shown in the diagram. Again, the 4×4 P matrix is solved, inverted, and multiplied with W to determine the amplitudes of the pulses A, B, C, and D which result in complete rephasing of static through pulsatile material.

It has been possible to significantly reduce motion artifacts and improve image quality by solving up to the third order for MAST sequence gradient waveform in the slice select and read axes.

REFERENCES

1. Ehman RL, McNamara MT, Pallack M, Hricak H, Higgins CB. Magnetic resonance imaging with respiratory gating: techniques and advantages. *AJR* 1984;143:1175–82.
2. Bailes DR, Gilderdale DJ, Bydder GM, Collins AG, Firmin DN. Technical note. Respiratory ordered phase encoding (ROPE): a method for reducing respiratory motion artefacts in MR imaging. *J Comput Assist Tomogr* 1985;9:835–8.
3. Haacke EM, Patrick JL. Reducing motion artifacts in two dimensional Fourier transform imaging. *Mag Res Imag* 1986;4:359–76.
4. Stark DD, Wittenberg J, Edelman RR, et al. Detection of hepatic metastases: analysis of pulse sequence performance in MR imaging. *Radiology* 1986;159:365–70.
5. Bailes DR, Young IR, Thomas DJ, Straughan K, Bydder GM, Steiner RE. NMR imaging of the brain using spin-echo sequences. *Clin Radiol* 1982;33:395–414.
6. Young IR, Bailes DR, Burl M, et al. Initial clinical evaluation of a whole body nuclear magnetic resonance (NMR) tomograph. *J Comput Assist Tomogr* 1982;6:1–18.
7. Bydder GM, Steiner RE, Blumgart LH, Khenia S, Young IR. MR imaging of the liver using short T1 inversion recovery sequences. *J Comput Assist Tomogr* 1985;9:1084–9.
8. Lee JK, Heiken JP, Dixon WT. Detection of hepatic metastases by proton spectroscopic imaging. Work in progress. *Radiology* 1985;156:429–33.
9. Reinig JW, Doppman JL, Dwyer AJ, Johnson AR, Knop RH. Distinction between adrenal adenomas and metastases using MR imaging. *J Comput Assist Tomogr* 1985;9:898–901.
10. Stark DD, Felder RC, Wittenberg J, et al. Magnetic resonance imaging of cavernous hemangioma of the liver: tissue-specific characterization. *AJR* 1985;145:213–22.
11. Hricak H. MRI of the female pelvis: a review. *AJR* 1986; 146:1115–22.
12. Winkler ML, Hricak H. Pelvis imaging with MR: technique for improvement. *Radiology* 1986;158:848–9.